https://doi.org/10.5194/acp-2019-916
Preprint. Discussion started: 29 October 2019
© Author(s) 2019. CC BY 4.0 License.

Atmospheric Chemistry and Physics Discussions

Characteristics, sources and reactions of nitrous acid during winter in the core city of the Central Plains Economic Region in China via high-time-resolution online measurements

Qi Hao, Nan Jiang*, Ruiqin Zhang, Liuming Yang, and Shengli Li

Key Laboratory of Environmental Chemistry and Low Carbon Technologies of Henan Province, Research Institute of Environmental Science, College of Chemistry, Zhengzhou University, Zhengzhou 450001, China

Abstract

Nitrous acid (HONO) in the core city of the Central Plains Economic Region was measured using an ambient ion monitor from January 9 to 31, 2019. Measurement time intervals were classified into the following periods in accordance with the daily mean values of $PM_{2.5}$: clean days (CD), pollution days (PD), and severe pollution days (SPD). The HONO concentrations during CD, PD, and SPD were 1.2, 2.3, and 3.7 ppbv, respectively. The contribution of the three sources varied under different pollution levels. The mean values of the net HONO production of the homogeneous reaction (P^{net}_{OH+NO}) in CD, PD, and SPD periods were 0.51, 1.03, and 2.18 ppbv h^{-1}, respectively. The average conversions of NO_2 (C_{HONO}) in CD, PD, and SPD periods were 0.72×10^{-2}, 0.64×10^{-2}, and 1.54×10^{-2} h^{-1}, respectively, indicating that the heterogeneous conversion of NO_2 was unimportant. Furthermore, the net production of the homogeneous reaction may have been the main factor for the increase in HONO under high-NO_X conditions (i.e., the concentration of NO was higher than that of NO_2) at nighttime. Daytime HONO budget analysis showed that the mean values of the unknown source ($P_{unknown}$) during CD, PD, and SPD periods were 0.26, 0.40, and 1.83 ppbv h^{-1}, respectively. The values of P^{net}_{OH+NO}, C_{HONO}, and $P_{unknown}$ in the SPD period were comparatively larger than those in other periods, indicating that HONO participated in many reactions. The proportions of nighttime HONO sources also changed

https://doi.org/10.5194/acp-2019-916
Preprint. Discussion started: 29 October 2019
© Author(s) 2019. CC BY 4.0 License.

Atmospheric Chemistry and Physics Discussions

during the entire sampling period. Direct emission and a heterogeneous reaction controlled HONO production in the first half of the night and provided a contribution larger than that of the homogeneous reaction. The proportion of homogenization gradually increased in the second half of the night due to the steady increase in NO concentration. The hourly abatement level of HONO abatement pathways, except for OH + HONO, should be at least 1.47 ppbv h^{-1} in the SPD period. The cumulative frequency distribution of the $HONO_{emission}$/HONO ratio (less than 20%) was approximately 76.7%, which suggests that direct emission was important. The heterogeneous HONO production increased when the relative humidity (RH) increased from 52% to 77%, but it decreased when RH increased further. The average $HONO/NO_X$ ratio (4.9%) was more than twice the assumed globally averaged value (2.0%).

1. Introduction

Nitrous acid (HONO) is important in the photochemical cycle and can provide hydroxyl radicals (OH):

$HONO + h\nu \rightarrow OH + NO$ ($300\ nm < \lambda < 405\ nm$) (R1).

According to measurement and simulation studies (Alicke et al., 2002), the contribution rate of HONO to OH radical concentration can reach 25%−50%, especially when the concentration of OH radicals produced by the photolysis of ozone and formaldehyde is relatively low (two to three hours after sunrise) (Czader et al., 2012). OH radical is also an important oxidant in the atmosphere, and it can react with organic substances, control the oxidation capacity of the atmosphere, and accelerate the formation of secondary aerosols in urban atmosphere (Sörgel et al., 2011). Therefore, reaction changes during pollution can be observed by studying the formation mechanism of HONO.

Several instruments have been used to determine ambient HONO concentrations, and these include differential optical absorption spectrophotometer (DOAS) (Winer and Biermann, 1994), long path absorption photometer (LOPAP) (Heland et al., 2001), Nitro-MAC (Michoud et al., 2014), stripping coil-UV/vis absorption photometer (SC-AP)

https://doi.org/10.5194/acp-2019-916
Preprint. Discussion started: 29 October 2019
© Author(s) 2019. CC BY 4.0 License.

Atmospheric Chemistry and Physics Discussions

(Pinto et al., 2014), and ambient ion monitor (AIM) (VandenBoer et al., 2014). A previous comparison of different instruments showed that SC-AP is compatible with two spectral measurement instruments, namely, LOPAP and DOAS (Pinto et al., 2014). Compared with HONO measured by SC-AP deployed onsite, HONO measured by AIM has a small error and is within the acceptable analytical uncertainty; the results exhibited a consistency of nearly 1:1 (VandenBoer et al., 2014). Previous studies have reported that HONO concentrations range from a few pptv in clean remote areas to several ppbv (0.1−2.1 ppbv) in air-polluted urban areas (Hou et al., 2016;Michoud et al., 2014).

The sources of HONO are direct emission and homogeneous and heterogeneous reactions (Acker et al., 2005;Grassian, 2001;Kurtenbach et al., 2001). HONO can be directly discharged into the atmosphere during vehicle operation and biomass combustion. Through a tunnel experiment, Kurtenbach et al. (2001) discovered that motor vehicles emit a small amount of HONO, and the HONO/NO_X ratio of HONO combustion sources (aside from NO_X and other pollutants) accounts for 0.1%–0.8% (Kurtenbach et al., 2001). Another study showed that the homogeneous reaction of NO and OH radicals is the major source of HONO under increased NO concentrations (Spataro et al., 2013). Furthermore, HONO can be absorbed by the OH radical (Alicke, 2003;Vogel et al., 2003). Tong et al. (2015) used NO + OH and HONO + OH homogeneous reactions, to calculate the net generation rate of HONO homogeneous reactions at night (Tong et al., 2015), which are expressed as:

$NO + OH \rightarrow HONO$ (R2);

$HONO + OH \rightarrow NO_2 + H_2O$ (R3).

Such calculations have been applied in studies on nighttime sources and daytime budgets (Hou et al., 2016;Huang et al., 2017). Finlayson-Pitts et al. (2003) studied mineral dust particles by using isotope-labeled water and revealed the mechanism of the reaction between adsorbed NO_2 and H ion dissociated from surface chemically adsorbed H_2O (Finlayson-Pitts et al., 2003):

https://doi.org/10.5194/acp-2019-916
Preprint. Discussion started: 29 October 2019
© Author(s) 2019. CC BY 4.0 License.

Atmospheric Chemistry and Physics Discussions

$2NO_2 + H_2O \rightarrow HONO + HNO_3$ (R4).

In China, most studies for HONO have concentrated on the Yangtze River Delta, Pearl River Delta and Jing-Jin-Ji region. For example, Hao et al. (2006) reported that field measurement results, especially HONO/NO_2 and relative humidity (RH), have a significant correlation and proved that heterogeneous reactions are an important source of nighttime HONO (Hao et al., 2006). Although the specific chemical mechanisms of heterogeneous reactions remain unknown, the intensity of HONO formation by NO_2 can be expressed by the HONO conversion frequency (Alicke et al., 2002;Li et al., 2012). Su et al. (2008a) revealed the importance of the OH radical from HONO during daytime (9:00–15:00 local time) and found that many unknown sources that are closely related to radiation lead to HONO formation (Su et al., 2008a). The researchers suggested that the method of budget analysis is crucial for obtaining the missing source. Spataro et al., (2013) measured the HONO level in Beijing's urban area and discussed the spatiotemporal changes, meteorological effects, and contributions of HONO from different sources. They used the measured HONO data to compare pollution periods in Beijing's urban and suburban areas. Tong et al. (2015) discovered that the possible mechanisms of HONO formation, namely, direct emission, heterogeneous formation, and homogeneous reaction, differ in the two sites. A few studies (Cui et al., 2018;Hou et al., 2016) compared the characteristics and sources of HONO during severe-pollution and clean periods. Although the definitions of the two periods are different, both can be used to analyze the diurnal variation, source, and daytime budget of HONO during the aggravation of pollution.

There is no study of HONO in the Central Plains Economic Region (CPER), with a total population of 0.18 billion by the end of 2011. CPER is the important region for food production and modern agriculture published by the Chinese government (http://www.ndrc.gov.cn/zcfb/zcfbtz/201212/P020121203614181974825.pdf), characterizing different influence factors for atmospheric pollution, including economic development level, energy structure, industrial structure, and geographic position (solar radiation)

https://doi.org/10.5194/acp-2019-916
Preprint. Discussion started: 29 October 2019
© Author(s) 2019. CC BY 4.0 License.

Atmospheric Chemistry and Physics Discussions

with the Yangtze River Delta, Pearl River Delta and Jing-Jin-Ji region. As the core city of the CPER, Zhengzhou is characterized by severe PM pollution (Jiang et al., 2017;Jiang et al., 2018d), selected in the study. In recent years, comprehensive PM research has been conducted on Zhengzhou's chemical characteristics (Jiang et al., 2018b;Li et al., 2019), source apportionment (Jiang et al., 2018c;Jiang et al., 2018e;Liu et al., 2019), health risks (Jiang et al., 2019a;Jiang et al., 2019b), and emission source profiles (Jiang et al., 2018a). However, no study has been performed on the sources and characteristics of HONO in Zhengzhou. Moreover, no synthetic research on different pollution levels in the area is available. In the current study, AIM was used to sample and analyze HONO concentrations. The interactions between HONO and other chemicals, such as $PM_{2.5}$, during pollution were assessed to understand the formation and removal of HONO and the influence on different pollution periods. This investigation of $PM_{2.5}$ and HONO is expected to clarify the sources, sinks, and reactions in fine PM pollution and the importance of systematic research. RH was also analyzed to provide a detailed understanding of HONO generation intensity under different RH conditions. Analysis of the sources of HONO at night provides strong support for conducting HONO budget analysis during daytime. To the best of the authors' knowledge, the formation characteristics of HONO at continuous and high time resolutions and different pollution levels have not been studied in Zhengzhou. This work can assist the governments of the CPER in formulating policy to decrease the level of HONO precursors, i.e., NO and NO_2, and HONO direct emission from vehicle.

2. Experiment and methods

2.1. Sampling site and period

The sampling site is on the rooftop (sixth floor) of a building in Zhengzhou University (34°48' N, 113°31' E), which is located in the northwestern part of Zhengzhou, China. The observation height is about 20 m from the ground, and the observation platform is relatively open without any tall buildings around. The site is close to the West Fourth Ring Road of Zhengzhou City and about 2 km from Lian Huo Expressway to

https://doi.org/10.5194/acp-2019-916
Preprint. Discussion started: 29 October 2019
© Author(s) 2019. CC BY 4.0 License.

Atmospheric Chemistry and Physics Discussions

the north. The measurement period was from January 9 to 31, 2019. Daily data were divided into two periods, namely, daytime (7:00–18:00 local time (Ammann et al.)) and nighttime (19:00–6:00 the next day, LT).

2.2. High-time-resolution instruments

AIM (URG-9000D, Thermo, USA), an online ion chromatographic monitoring system for particle and gas components in the atmosphere, was used to measure HONO concentration continuously at a temporal resolution of 1 h. The atmospheric airflow entered the $PM_{2.5}$ cyclone cutting head through the sample tube, and gas–solid separation was performed with a parallel plate denuder with a new synthetic polyamide membrane. The denuder had no moving parts and could be changed without stopping the sampler. The conversion of gas samples from the atmospheric environment is shown in **Fig. S1**. HONO was absorbed by the denuder with an absorption liquid (5.5 mM H_2O_2). **Fig. S2** presents the specific process of gas dissolution in the denuder. The substances that could be oxidized were absorbed by H_2O_2 on the porous membrane surface, but several gases (e.g., O and N) were expelled by the air pump. The abundance of other gaseous acids and bases affected the efficiency of HONO collection by AIM due to the relation between Henry's law constant and pH. This measurement method and its details have been successfully evaluated in many field studies (Markovic et al., 2012;Tian et al., 2018;Wang et al., 2019). In addition, a QXZ1.0 automatic weather station (Yigu Technologies, China) was used for synchronous observation of meteorological parameters, including temperature (T), RH, wind direction (WD), and wind speed (WS). O_3, CO, NO, NO_X, NO_2, and $PM_{2.5}$ were measured with a model analyzer (TE, 48i, and 42i, Thermo, USA) and TEOM 1405 $PM_{2.5}$ monitor (Thermo Electron, USA) with a temporal resolution of 1 h. Detailed information can be found in the work of (Wang et al., 2019).

During the sampling period, all instruments were subjected to strict quality control to avoid possible contamination. The instrument accessories and sampling process were

https://doi.org/10.5194/acp-2019-916
Preprint. Discussion started: 29 October 2019
© Author(s) 2019. CC BY 4.0 License.

Atmospheric Chemistry and Physics Discussions

periodically replaced and calibrated, respectively. The instrument parts and consumables should be changed regularly during the observation process, and the sampling flow should be calibrated to reduce the negative effect of accessories on sampling. The membrane of the denuder was replaced every six weeks. Standard anion and cation solutions were prepared every two months, and the standard curve was drawn to ensure the appropriateness of the correlation coefficient ($\geqslant$0.999) and the accuracy of the sample retention time and response value. The minimum detection limit of AIM was 0.004 ppbv. Other detailed information can be found in the work of (Wang et al., 2019).

3. Results and Discussion

3.1. Temporal variations of meteorological parameters and pollutants

The daily changes in meteorological parameters and $PM_{2.5}$ are shown in **Fig. 1**. In accordance with the daily average concentration level of $PM_{2.5}$, the analysis and measurement process was divided into three periods (clean days [CD], pollution days [PD], and severe pollution days [SPD]). The days wherein the daily averages of $PM_{2.5}$ were lower than the second grade in China National Ambient Air Quality Standards (CNAAQS) (75 μg m^{-3}) (Zhang et al., 2019) represented CD (January 9, 16, 17, 21, 22, 23, 26, and 31), with RH ranging from 4.6% to 78.9% and WS ranging from 0 m s^{-1} to 4.2 m s^{-1}. The days wherein the daily averages of $PM_{2.5}$ were between 75 and 115 μg m^{-3} represented PD (January 10, 15, 18, 20, 25, 27, and 28), with RH ranging from 17.1% to 86.3% and WS ranging from 0 m s^{-1} to 4.6 m s^{-1}. The days wherein the daily averages of $PM_{2.5}$ were higher than 115 μg m^{-3} represented SPD (January 11, 12, 13, 14, 19, 24, 29 and 30), with RH ranging from 30.3% to 96.1% and WS ranging from 0 m s^{-1} to 3.5 m s^{-1}. Northwest or east wind was observed in most of the observation periods, except for January 21–22. The WD was north, WS was high, the $PM_{2.5}$ concentration decreased rapidly, and the effect of pollution removal was evident. **Table 2** lists the data statistics of HONO, $PM_{2.5}$, NO_2, NO, NO_X, HONO/NO_2, HONO/NO_X, O_3, CO, T, RH, WS, and WD during the measurement period together with their mean value ± standard deviation. The meteorological parameters in **Table 2** show that the average

https://doi.org/10.5194/acp-2019-916
Preprint. Discussion started: 29 October 2019
© Author(s) 2019. CC BY 4.0 License.

Atmospheric Chemistry and Physics Discussions

RH in CD, PD, and SPD periods was 32.8%, 48.6%, and 68.3%, respectively. In SPD, RH was high and WD was low (mean value of 0.4 m s^{-1}).

In accordance with the data on trace gases, the average HONO values in CD, PD, and SPD were 1.1, 2.3, and 3.7 ppbv, respectively. The mean values of NO_2 were 24.6, 33.2, and 41.7 ppbv (46.2, 62.7, and 78.4 μg m^{-3} lower than the first grade in CNAAQS [80 μg m^{-3}]), respectively. The mean values of CO were 0.8, 1.3, and 1.8 ppmv (0.9, 1.5, and 2.1 mg m^{-3} lower than the first grade in CNAAQS [4 mg m^{-3}]), respectively. The variations of the average HONO, $PM_{2.5}$, NO_2, and CO in the three periods were similar. The mean values in the SPD period were the largest, and those in the CD period were the smallest. The highest mean value of O_3 occurred in the CD period, similar to previous observations (Hou et al., 2016;Huang et al., 2017;Zhang et al., 2019).

Fig. 2 shows the concentration changes in HONO and gas species throughout the measurement period. The HONO concentrations ranged from 0.2 ppbv to 14.8 ppbv and had an average of 2.5 ppbv, which is higher than the average values of 0.6 (Rappenglück et al., 2013), 1.5 (Hou et al., 2016), and 1.0 ppbv (Huang et al., 2017) in previous urban studies. The diurnal variations of HONO, NO, NO_2, O_3, HONO/NO_2, and HONO/NO_X are illustrated in **Fig. 3**. After sunset, the HONO concentrations in CD, PD, and SPD began to accumulate due to the attenuation of solar radiation and the stabilization of the boundary layer (Cui et al., 2018). The maximum values of 1.7, 4.1, and 6.9 ppbv were reached in the morning (08:00–10:00 LT) in CD, PD, and SPD, respectively. After sunrise, the HONO concentration decreased because of the increased solubility and rapid photolysis then remained at a low level before sunset (14:00–16:00 LT). The diurnal variations of HONO during the measurement were similar in the three periods, as shown in **Fig. S3**. The NO and NO_2 concentration increased in the morning rush hours, decreased rapidly afterward, and remained low in the afternoon. After sunset, the concentrations of NO and NO_2 began to increase again and remained at a high level after midnight until sunrise. Furthermore, the diurnal variation of NO in the CD period was similar to that of NO_2. The peak was reached at around 09:00 LT due to

https://doi.org/10.5194/acp-2019-916
Preprint. Discussion started: 29 October 2019
© Author(s) 2019. CC BY 4.0 License.

Atmospheric Chemistry and Physics Discussions

vehicle emission in the morning rush hours, and the lowest value was observed at around 16:00 LT. After 18:00 LT, the boundary layer height decreased in the evening rush hours, resulting in an increase in NO and NO_2 concentrations (Hendrick et al., 2014). O_3 showed a diurnal cycle and had maximum values in CD, PD, and SPD periods in the afternoon. The HONO/NO_2 ratio is commonly used to estimate the formation of HONO in NO_2 transformation (Wang et al., 2013). Compared with HONO formation, NO_2 transformation is less affected by diffusion during atmospheric migration (Li et al., 2012). The HONO/NO_2 ratio in the CD period began to increase after sunset and reached its peak at night. Then, it decreased in the morning as a result of the enhancement of NO_2 emission and photolysis of HONO. However, the mean value of HONO/NO_2 in PD and SPD periods gradually increased from nighttime and eventually reached the maximum values of 14.3% and 18.9% at 09:00 and 10:00 LT, respectively. This result indicates that the strength of the heterogeneous reaction increased slightly with the exacerbation of pollution. The HONO/NO_2 ratio showed a diurnal cycle with a low level in the afternoon and a high level after sunset due to the heterogeneous reaction of NO_2 on the ground and aerosol surface (Su et al., 2008b). For comparison, the daytime and nighttime HONO, HONO/NO_2, and HONO/NO_X mean values in other cities around the world are listed in **Table 1**. The values of HONO, HONO/NO_2, and HONO/NO_X in Zhengzhou are relatively higher than those in other parts of the world.

3.2. Nocturnal HONO sources and formation

3.2.1. Homogeneous reaction of NO and OH

The homogeneous reaction of NO and OH (R2 and R3) is the main pathway of HONO formation in the gas phase. Spataro et al. (2013) found that the formation mechanism leads to an increase in HONO in high-pollution areas with an increase in NO at night (Spataro et al., 2013). P^{net}_{OH+NO} can be understood as the net hourly HONO production amount of homogeneous reaction and is calculated as

$$P^{net}_{OH+NO} = k_{OH+NO}\,[OH][NO] - k_{OH+HONO}\,[OH][HONO] \quad (2)$$

At T=298 K and P=101 kPa, the rate constants of k_{OH+NO} and $k_{OH+HONO}$ are

https://doi.org/10.5194/acp-2019-916
Preprint. Discussion started: 29 October 2019
© Author(s) 2019. CC BY 4.0 License.

Atmospheric Chemistry and Physics Discussions

9.8×10^{-12} and 6.0×10^{-12} cm^3 $molecule^{-1}$ s^{-1}, respectively. [OH] is the concentration of OH radicals that cannot be obtained in the measurement. Therefore, in reference to Beijing, the average value of OH measured in Zhengzhou at night can be assumed to be 1.0×10^6 cm^3 $molecule^{-1}$ (Lelieveld et al., 2016). P^{net}_{OH+NO} primarily depends on the concentrations of NO and HONO because the reaction rates of k_{OH+NO} and $k_{OH+HONO}$ are close. **Fig. 4** shows the nocturnal variations of P^{net}_{OH+NO}, NO, and HONO during CD, PD, and SPD periods. When the NO levels were high, the variations of P^{net}_{OH+NO} followed those of NO during the three periods (Atkinson et al., 2004). The mean value of P^{net}_{OH+NO} was 1.31 ppbv h^{-1}, and the specific values in CD, PD, and SPD periods were 0.51, 1.03, and 2.18 ppbv h^{-1}, respectively.

P^{net}_{OH+NO} varied from 0.04 ppbv h^{-1} to 1.89 ppbv h^{-1} during the CD period. The mean value of P^{net}_{OH+NO} increased before midnight, decreased after midnight, and increased slightly at 3 am. In the PD period, P^{net}_{OH+NO} ranged from 0.26 ppbv h^{-1} to 1.74 ppbv h^{-1}. The situation was similar to that in the CD period, except that the value remained almost constant. In addition, the contribution of HONO from homogeneous reaction during the SPD period was larger than those in the CD and PD periods, and the level of P^{net}_{OH+NO}, with an average value of 2.18 ppbv h^{-1}, was equal to the value in a previous study (2.18 ppbv h^{-1} in Beijing) (Tong et al., 2015). From 19:00 LT to 03:00 LT, the mean value of P^{net}_{OH+NO} increased from 0.59 ppbv h^{-1} to 3.60 ppbv h^{-1}. HONO increased from 2.84 ppbv to 4.59 ppbv and subsequently decreased to 4.43 ppbv. By integrating P^{net}_{OH+NO} during the eight hours, the homogeneous reaction can provide an accumulated HONO formation of at least 13.41 ppbv (i.e., 0.59 + 0.79 + 1.01 + 1.03 + 1.38 + 2.21 + 2.80 + 3.60 ppbv). However, the mean accumulation value of measured HONO in this nighttime period was merely 1.59 ppbv. With the increase in pollution level, the HONO accumulation time at nighttime increased. This result indicates that first, the homogeneous reaction of OH + NO is sufficient to augment HONO in the first half of the night, although NO_2 transformation and other sources may still exist. When the concentration of NO is relatively high, the net production generated by OH + NO

https://doi.org/10.5194/acp-2019-916
Preprint. Discussion started: 29 October 2019
© Author(s) 2019. CC BY 4.0 License.

Atmospheric Chemistry and Physics Discussions

may be the leading factor for the increase in HONO at night (Tong et al., 2015). Second, the hourly abatement level of HONO abatement pathways, except OH + HONO, should be at least 1.47 ppbv h^{-1} (i.e., 13.41 – 1.59 ppbv) / 8 h). The contributions of other HONO abatement pathways in the current work even exceeded the formation of heterogeneous reactions, similar to a previous study (Spataro et al., 2013).

3.2.2. Direct emission

At present, no HONO emission inventory or emission factor database for Zhengzhou is available. As a result, estimating any HONO from direct emission is difficult. In the current study, directly emitted HONO could have been generated by vehicle exhaust and biomass combustion because no pollution source was near the measurement site. Hence, only night data (17:00–06:00 LT) were considered to avoid the problem of instant photolysis of directly emitted HONO. In a previous study, the HONO/NO_X ratio from tunnel measurement was set to 0.65% to estimate an upper limit of HONO emitted by traffic near the site (Kurtenbach et al., 2001). The minimum value of HONO/NO_X in the SPD period in the current work was 1.5%, which is slightly higher than the value measured in the abovementioned study. Directly emitted HONO at night was not transformed immediately. The HONO concentrations corrected by direct emissions are given as

$$[HONO]_{correct} = [HONO] - [HONO]_{emission} = [HONO] - 0.0065 \times [NO_X], \quad (2)$$

where $[HONO]_{emission}$, $[NO_X]$, and 0.0065 are direct emission HONO concentration, NO_X concentration, and HONO/NO_2 direct emission ratio, respectively. The direct emission contribution was estimated by comparing the direct emission HONO with the observed HONO. The ranges of $HONO_{emission}$/HONO in CD, PD, and SPD periods were 2%–52%, 6%–34%, and 2%–41%, respectively, and the mean values were 17%, 16%, and 16%, respectively. The frequency distribution of the $HONO_{emission}$/HONO ratio at nighttime is shown in **Fig. 5**. For this upper limit estimation, the frequency distribution of $HONO_{emission}$/HONO (less than 20%) was approximately 76.7%. Hence, direct emission may not be the main reason for the high growth of HONO levels. Compared with

https://doi.org/10.5194/acp-2019-916
Preprint. Discussion started: 29 October 2019
© Author(s) 2019. CC BY 4.0 License.

Atmospheric Chemistry and Physics Discussions

the direct emission of other sites, that of the measurement site accounted for a lower proportion possibly because the site is relatively far from the highway in the campus.

3.2.3. Heterogeneous conversion of NO_2 to HONO

NO_2 is an important precursor for HONO formation. In addition, recent field measurements in many urban locations have shown that a positive correlation exists between HONO and NO_2 (Cui et al., 2018;Hao et al., 2006;Huang et al., 2017;Zhang et al., 2019), suggesting they have a common source. Moreover, (Acker et al., 2005) reported that different meteorological conditions may lead to significant differences in the relationship between the source and receptor, and these differences lead to various types of correlation. During the measurement period, the HONO/NO_2 ratio varied between 1.3% and 59.0%, with an average of 7.6%, which is slightly higher than the 6.2% average in a previous study (Cui et al., 2018). The HONO/NO_2 ratio calculated in this work is much larger than that calculated for direct emission (< 1%) (Kurtenbach et al., 2001), suggesting that heterogeneous reactions may be a more important pathway for HONO production than direct emissions. With regard to the heterogeneous conversion of NO_2, several studies (An et al., 2012;Shen and Zhang, 2013) have reported that the surface of soot particles is the medium. The contribution of soot surface to HONO production is usually much lower than expected because the uptake efficiency of NO_2 decreases with the prolonged reaction time caused by surface deactivation. The aerosol surface is an important medium for the heterogeneous transformation from NO_2 to HONO (Liu et al., 2014). The mass concentration of aerosols was used as an alternative to identify the influence of aerosols in this study because the surface density of aerosols could not be obtained.

The correlations between $PM_{2.5}$ and HONO/NO_2 ratio in CD, PD, and SPD periods are shown in **Fig. 6**. With the exacerbation of the $PM_{2.5}$ level,

https://doi.org/10.5194/acp-2019-916
Preprint. Discussion started: 29 October 2019
© Author(s) 2019. CC BY 4.0 License.

Atmospheric Chemistry and Physics Discussions

the average value of $HONO/NO_2$ gradually increased, indicating that the aerosol surface occupied an important position in the heterogeneous transformation. Comparison of $HONO/NO_2$ and HONO with $PM_{2.5}$ showed that the correlation between $HONO/NO_2$ and $PM_{2.5}$ (R^2=0.23) was weaker than that between HONO and $PM_{2.5}$ (R^2=0.55) in the entire period. The main source of HONO could not have been the transformation of NO_2. Notably, the HONO correlation in the PD period was significantly stronger than that in the two other periods. This result proves that HONO-related reactions occurred more frequently during this period. The increased HONO in ambient air during the pollution period could have been caused by the comparatively high loading and large particle surface (Cui et al., 2018). Similar phenomena have been observed in a correlation study on CO and HONO wherein CO was used as a tracer for traffic-induced emissions and tested by considering the correlation between HONO and CO over an identical time interval (Qin et al., 2009). The correlation coefficient between HONO and CO was relatively moderate (R^2=0.43), indicating that HONO and CO processes affected most cases.

The absorbed water influenced the heterogeneous formation (Stutz et al., 2004). The influence of RH on the heterogeneous conversion is shown in **Fig. 6(d)**. When RH was less than 52%, the $HONO/NO_2$ ratio slowly increased. When RH was greater than 52% but less than 77%, the $HONO/NO_2$ ratio began to increase rapidly with RH. The $HONO/NO_2$ ratio decreased when RH was further increased. Similar variation patterns have been obtained in previous studies (Huang et al., 2017;Qin et al., 2009;Tong et al., 2015). Surface adsorbed water functions not only as sources but also as sinks of HONO by affecting the hydrolysis of NO_2 and the sedimentation of HONO to generate HONO (Ammann et al., 1998). When RH ranged from 52%

https://doi.org/10.5194/acp-2019-916
Preprint. Discussion started: 29 October 2019
© Author(s) 2019. CC BY 4.0 License.

Atmospheric Chemistry and Physics Discussions

to 77%, the moisture effect of HONO was more severe than that of sedimentation. This phenomenon confirms that RH improved the conversion efficiency (Stutz et al., 2004). However, the surface reached saturation when RH was greater than 77%. The excess water restricted NO_2 transformation (Wojtal et al., 2011). The absorption and dissolution of HONO by the saturated surface water layer caused $HONO/NO_2$ ratio to decrease drastically.

The study of the correlation between $HONO_{correct}$ and NO_2 at nighttime is shown in **Fig. S4**. $HONO_{correct}$ was used in the calculation to exclude the influence of direct emission on NO_2 conversion. The nocturnal variations of $HONO_{correct}$, NO_2, and $HONO_{correct}/NO_2$ ratios in the CD, PD, and SPD periods are presented in **Fig. 7**. In general, the $HONO_{correct}/NO_2$ ratio reached its maximum at or before midnight but decreased after midnight. In the PD and SPD periods, HONO was generated by heterogeneous reaction (R4), and NO_2 decreased. The production of HONO was equal to its loss (mainly night deposition), and HONO concentration reached a relatively stable state (Stutz, 2002). The weak correlation between nighttime $HONO/NO_2$ and $PM_{2.5}$ can be reasonably explained by the stable $HONO_{correct}/NO_2$ ratio after midnight (Qin et al., 2009). A previous study (Xu et al., 2015) found that a low $HONO_{correct}$ in the first half of the night (19:00–00:00 LT) indicates an important contribution of automobile exhaust emissions, and a low $HONO_{correct}$ in the second half of the night means heterogeneous reactions dominate. Therefore, the heterogeneous reaction conversion rate of HONO was calculated in then current study by using the data of $HONO_{correct}$.

The conversion rate of HONO (C_{HONO}) is usually used as an indicator to test the efficiency of NO_2 heterogeneous reactions. Total $HONO_{correct}$ was assumed to be generated by the heterogeneous transformation of NO_2. The formula for the conversion rate of NO_2 (C_{HONO}) is as follows (Su et al., 2008a;Xu et al., 2015):

https://doi.org/10.5194/acp-2019-916
Preprint. Discussion started: 29 October 2019
© Author(s) 2019. CC BY 4.0 License.

Atmospheric Chemistry and Physics Discussions

$$C_{HONO}=([HONO_{correct}]_{t2} - [HONO_{correct}]_{t1}) / (t2 - t1)\,[NO_2], \quad (3)$$

where $[NO_2]$ is the average concentration of NO_2 within the t2–t1 time interval (1 h). In this study, the average conversion rate of NO_2 was 1.02×10^{-2} h^{-1}. The mean values of C_{HONO} in the CD, PD, and SPD periods were 0.72×10^{-2}, 0.64×10^{-2}, and 1.54×10^{-2} h^{-1}, respectively. The conversion rates in this study were 0.58×10^{-2} and 1.46×10^{-2} h^{-1} higher than those of Beijing I (polluted) and II (heavily polluted) periods, respectively. The improvement of the conversion rate demonstrates that NO_2 had high reaction efficiency through the process from NO_2 to HONO in the aggravation of pollution, which could have led to the high utilization efficiency of the aerosol surface due to good particle surface properties (e.g., surface type and moisture).

3.3. Daytime HONO budget

$\frac{d\,HONO}{d\,t}$ represents the observed variations of hourly HONO concentrations, for which we can use $\Delta HONO/\Delta dt$ instead. $P_{unknown}$ is the production rate by an unknown daytime HONO source. P_{OH+NO} is the rate of reaction of NO and OH. P_{emi} represents the direct emission rate of HONO from combustion processes. The heterogeneous transformation mechanism was assumed to be the same for day and night. Therefore, the daytime heterogeneous productivity ($P_{het}= C_{HONO} \times [NO_2]$) was calculated with the nighttime mean values of C_{HONO} in the different periods. $L_{OH+HONO}$ is the rate of the reaction between OH and HONO (R3). The calculation formulas of P_{OH+NO} and $L_{OH+HONO}$ have been provided in **Section 3.2.1**. Upon sunlight irradiation, an OH radical and NO were formed as R1. L_{photo} represents the photolysis loss rate of HONO ($L_{photo} = J_{HONO} \times [HONO]$). The photolysis frequency and OH radical concentration could not be directly measured in this study. Therefore, the tropospheric ultraviolet and visible (TUV) transfer model of the National Center for Atmospheric Research

https://doi.org/10.5194/acp-2019-916
Preprint. Discussion started: 29 October 2019
© Author(s) 2019. CC BY 4.0 License.

Atmospheric Chemistry and Physics Discussions

(http://cprm.acom.ucar.edu/Models/TUV/Interactive_TUV/) (Hou et al., 2016) was used to calculate the J_{HONO} value. The concentration of OH radicals was calculated with the formulas of NO_2, O_3, and J_{O^1D} (Rohrer and Berresheim, 2006). Aerosol effects were considered by using aerosol optical thickness (AOD), single scattering albedo (SSA), and Angstrom exponent as inputs in the TUV model. Typical AOD, SSA, and Angstrom exponent values of 1.32, 0.9, and 1.3, respectively, were adopted for the PD and SPD periods. In the CD period, the respective values were 0.66, 0.89, and 1.07 (Che et al., 2015;Cui et al., 2018;Hou et al., 2016). The average profiles of J_{HONO} and J_{O^1D} concentrations in the CD, PD, and SPD periods are shown in **Fig. 8**. The mean values of J_{HONO} and OH radical concentration in the CD, PD, and SPD periods were 5.93×10^{-4}, 3.79×10^{-4}, and 3.79×10^{-4} cm^3 $molecule^{-1}$ s^{-1} and 4.10×10^6, 2.93×10^6, and 3.76×10^6 cm^3 $molecule^{-1}$ s^{-1}, respectively. The results of the calculated OH radicals ranged from $(0.58-11.49)\times10^6$ cm^3 $molecule^{-1}$ s^{-1}, and the mean value was 3.57×10^6 cm^3 $molecule^{-1}$ s^{-1} at noon in Zhengzhou.

By studying the source and reduction, the daytime HONO budget was analyzed with Eq. (4) (Su et al., 2008b).

$$\frac{d\,HONO}{d\,t} = sources - sinks$$

$$= (P_{unknown} + P_{OH+NO} + P_{emi} + P_{het}) - (L_{OH+HONO} + L_{photo}) \quad (4)$$

$$P_{OH+NO} = k_{OH+NO}\,[OH]\,[NO] \quad (5)$$

$$L_{OH+HONO} = k_{OH+HONO}\,[OH]\,[HONO] \quad (6)$$

Each production and loss rate of daytime HONO during CD, PD, and SPD periods are illustrated in **Fig. 8** together with dHONO/dt. $P_{unknown}$ was at a high level before midday. $P_{unknown}$ approached 0 ppbv after midday. In the CD, PD, and SPD periods, the mean values of $P_{unknown}$ were 0.26, 0.40, and 1.83 ppbv h^{-1}, respectively; the mean values of P_{OH+NO} were 1.14, 2.07, and 4.03 ppbv h^{-1}, respectively; the mean values of P_{emi} were 0.17, 0.30, and 0.43

https://doi.org/10.5194/acp-2019-916
Preprint. Discussion started: 29 October 2019
© Author(s) 2019. CC BY 4.0 License.

Atmospheric Chemistry and Physics Discussions

ppbv h^{-1}, respectively; and the mean values of P_{het} were 0.14, 0.18, and 0.55 ppbv h^{-1}, respectively. The midday time $P_{unknown}$ (1.83 ppbv h^{-1}) calculated in Zhengzhou during the winter haze pollution period was close to the result obtained from Beijing's urban area (Hou et al., 2016) (1.85 ppbv h^{-1}). The $P_{unknown}$ contribution to daytime HONO sources in CD, PD, and SPD periods accounted for 15%, 14%, and 28% of the HONO production rate ($P_{unknown} + P_{OH+NO} + P_{emi} + P_{het}$), respectively. Previous studies (Spataro et al., 2013;Yang et al., 2014) have shown that meteorological conditions, such as solar radiation and WS, can affect unknown sources. The low $P_{unknown}$ contribution of daytime HONO concentration may be related to the low solar radiation and low wind speed during severe pollution. Although the values of P_{OH+NO} had high uncertainty because of the NO concentrations, P_{OH+NO} contributed the most to HONO production during daytime. In addition to the photolysis of HONO and the homogeneous reaction of HONO and OH, one or more important sinks might exist to control the variation between the sources and sinks of the daytime HONO during complex contamination. However, further research is needed to analyze the unknown sources of daytime HONO.

4. Conclusions

Ambient HONO measurement using AIM with other atmospheric pollutants and meteorological parameters was conducted in the CPER. The HONO concentrations during the entire measurement varied from 0.2 ppbv to 14.8 ppbv, with an average of 2.5 ppbv. The HONO concentrations in the CD, PD, and SPD periods were 1.1, 2.3, and 3.7 ppbv, respectively, and the HONO/NO_2 ratios were 4.7%, 7.1%, and 9.4%, respectively. HONO concentration was a combined action of direct emission and heterogeneous reaction, and the contributions of the two were higher than that of homogeneous reaction in the first half of the night. However, the proportion of homogenization gradually increased in the second half of the night due to the steady increase in NO concentration. The hourly abatement level of other HONO abatement pathways aside from OH + HONO should be at least 1.47 ppbv h^{-1} in the SPD period.

https://doi.org/10.5194/acp-2019-916
Preprint. Discussion started: 29 October 2019
© Author(s) 2019. CC BY 4.0 License.

Atmospheric Chemistry and Physics Discussions

The sum of the frequency distributions of the $HONO_{emission}$/HONO ratio less than 20% was approximately 76.7%, indicating that the direct emission of HONO was the main source of the observed HONO level at night. The mean values of $HONO_{emission}$/HONO in the CD, PD, and SPD periods were 17%, 16%, and 16%, respectively. This phenomenon means that the policy of restricting motor vehicles published by the local government in January 2019 had a good effect on decreasing HONO emissions. In addition, when RH increased from 52% to 77%, the heterogeneous HONO production increased, but it decreased when RH increased further due to the effect of surface water. The contribution of the three sources varied with different pollution levels. The mean values of C_{HONO} in the CD, PD, and SPD periods were 0.72×10^{-2}, 0.64×10^{-2}, and 1.54×10^{-2} h^{-1}, respectively. At nighttime in the SPD period, the heterogeneous conversion of NO_2 appeared to be unimportant. Furthermore, the net production generated by homogeneous reaction may be the leading factor for the increase in HONO under high-NO_X conditions (i.e., the concentration of NO was relatively higher than that of NO_2) at nighttime. The mean value of P^{net}_{OH+NO} in the CD, PD, and SPD periods were 0.51, 1.03, and 2.18 ppbv h^{-1}, respectively. Daytime HONO budget analysis showed that the mean values of $P_{unknown}$ in the CD, PD, and SPD periods were 0.26, 0.40, and 1.83 ppbv h^{-1}, respectively. Although the values of P_{OH+NO} had high uncertainty because of the variation of NO concentrations, P_{OH+NO} contributed the most to HONO production during daytime. After the analysis, C_{HONO}, P^{net}_{OH+NO}, and $P_{unknown}$ in the SPD period were larger than those in the other periods, indicating that HONO participated in many reactions.

Acknowledgements

The study was supported by the financial support from the National Natural Science Foundation of China (51808510, 51778587), National Key Research and Development Program of China (2017YFC0212400), Natural Science Foundation of Henan Province of China (162300410255).

https://doi.org/10.5194/acp-2019-916
Preprint. Discussion started: 29 October 2019
© Author(s) 2019. CC BY 4.0 License.

Atmospheric Chemistry and Physics Discussions

Reference

Acker, K., Möller, D., Auel, R., Wieprecht, W., and Kalaß, D.: Concentrations of nitrous acid, nitric acid, nitrite and nitrate in the gas and aerosol phase at a site in the emission zone during ESCOMPTE 2001 experiment, ATMOS RES, 74, 507-524, https://doi.org/10.1016/j.atmosres.2004.04.009, 2005.

Alicke, B., Platt, U., and Stutz, J.: Impact of nitrous acid photolysis on the total hydroxyl radical budget during the Limitation of Oxidant Production/Pianura Padana Produzione di Ozono study in Milan, J. Geophys. Res., https://doi.org/10.1029/2000jd000075, 2002.

Alicke, B.: OH formation by HONO photolysis during the BERLIOZ experiment, J. Geophys. Res., 108, https://doi.org/10.1029/2001jd000579, 2003.

Ammann, M., Kalberer, M., Jost, D. T., Tobler, L., Rössler, E., Piguet, D., Gäggeler, H. W., and Baltensperger, U.: Heterogeneous production of nitrous acid on soot in polluted air masses, Nature, 395, 157-160, https://doi.org/10.1038/25965, 1998.

An, J., Li, Y., Chen, Y., Li, J., Qu, Y., and Tang, Y.: Enhancements of major aerosol components due to additional HONO sources in the North China Plain and implications for visibility and haze, ADV ATMOS SCI, 30, 57-66, https://doi.org/10.1007/s00376-012-2016-9, 2012.

Atkinson, R., Baulch, D. L., Cox, R. A., Crowley, J. N., Hampson, R. F., Hynes, R. G., Jenkin, M. E., Rossi, M. J., and Troe, J.: Evaluated kinetic and photochemical data for atmospheric chemistry: Volume I - gas phase reactions of Ox, HOx, NOx and SOx species, ATMOS CHEM PHYS, 4, 1461-1738, https://doi.org/10.5194/acp-4-1461-2004, 2004.

Che, H., Xia, X., Zhu, J., Wang, H., Wang, Y., Sun, J., Zhang, X., and Shi, G.: Aerosol optical properties under the condition of heavy haze over an urban site of Beijing, China, Environ Sci Pollut Res, 22, 1043-1053, https://doi.org/10.1007/s11356-014-3415-5, 2015.

https://doi.org/10.5194/acp-2019-916
Preprint. Discussion started: 29 October 2019
© Author(s) 2019. CC BY 4.0 License.

Atmospheric Chemistry and Physics Discussions

526 Cui, L., Li, R., Zhang, Y., Meng, Y., Fu, H., and Chen, J.: An observational study of
527 nitrous acid (HONO) in Shanghai, China: The aerosol impact on HONO formation
528 during the haze episodes, Sci. Total Environ., 630, 1057-1070,
529 https://doi.org/10.1016/j.scitotenv.2018.02.063, 2018.
530 Czader, B. H., Rappenglück, B., Percell, P., Byun, D. W., Ngan, F., and Kim, S.:
531 Modeling nitrous acid and its impact on ozone and hydroxyl radical during the
532 Texas Air Quality Study 2006, ATMOS CHEM PHYS, 12, 6939-6951,
533 https://doi.org/10.5194/acp-12-6939-2012, 2012.
534 Finlayson-Pitts, B. J., Wingen, L. M., Sumner, A. L., Syomin, D., and Ramazan, K.
535 A.: The heterogeneous hydrolysis of NO2 in laboratory systems and in outdoor and
536 indoor atmospheres: An integrated mechanism, PCCP, 5, 223-242,
537 https://doi.org/10.1039/b208564j, 2003.
538 Grassian, V. H.: Heterogeneous uptake and reaction of nitrogen oxides and volatile
539 organic compounds on the surface of atmospheric particles including oxides,
540 carbonates, soot and mineral dust: Implications for the chemical balance of the
541 troposphere, Int. Rev. Phys. Chem., 20, 467-548,
542 https://doi.org/10.1080/01442350110051968, 2001.
543 Hao, N., Zhou, B., Chen, D., and Chen, L.: Observations of nitrous acid and its
544 relative humidity dependence in Shanghai, J ENVIRON SCI-CHINA, 18, 910-915,
545 https://doi.org/10.1016/s1001-0742(06)60013-2, 2006.
546 Harrison, R. M., Peak, J. D., and Collins, G. M.: Tropospheric cycle of nitrous acid, J.
547 Geophys. Res., 101, 14429-14439, https://doi.org/10.1029/96jd00341, 1996.
548 Heland, J., Kleffmann, J., Kurtenbach, R., and Wiesen, P.: A new instrument to
549 measure gaseous nitrous acid (HONO) in the atmosphere, Environ. Sci. Technol.,
550 35, 3207-3212, https://doi.org/10.1021/es000303t, 2001.
551 Hendrick, F., Müller, J. F., Clémer, K., Wang, P., De Mazière, M., Fayt, C., Gielen, C.,
552 Hermans, C., Ma, J. Z., Pinardi, G., Stavrakou, T., Vlemmix, T., and Van
553 Roozendael, M.: Four years of ground-based MAX-DOAS observations of HONO

https://doi.org/10.5194/acp-2019-916
Preprint. Discussion started: 29 October 2019
© Author(s) 2019. CC BY 4.0 License.

554 and NO_2 in the Beijing area, ATMOS CHEM PHYS, 14, 765-781,
555 https://doi.org/10.5194/acp-14-765-2014, 2014.
556 Hou, S., Tong, S., Ge, M., and An, J.: Comparison of atmospheric nitrous acid during
557 severe haze and clean periods in Beijing, China, Atmos. Environ., 124, 199-206,
558 https://doi.org/10.1016/j.atmosenv.2015.06.023, 2016.
559 Huang, R. J., Yang, L., Cao, J., Wang, Q., Tie, X., Ho, K. F., Shen, Z., Zhang, R., Li,
560 G., Zhu, C., Zhang, N., Dai, W., Zhou, J., Liu, S., Chen, Y., Chen, J., and O'Dowd,
561 C. D.: Concentration and sources of atmospheric nitrous acid (HONO) at an urban
562 site in Western China, Sci. Total Environ., 593-594, 165-172,
563 https://doi.org/10.1016/j.scitotenv.2017.02.166, 2017.
564 Jiang, N., Guo, Y., Wang, Q., Kang, P., Zhang, R., and Tang, X.: Chemical
565 composition characteristics of $PM_{2.5}$ in three cities in Henan, Central China,
566 AEROSOL AIR QUAL RES, 17, 2367-2380,
567 https://doi.org/10.4209/aaqr.2016.10.0463, 2017.
568 Jiang, N., Dong, Z., Xu, Y., Yu, F., Yin, S., Zhang, R., and Tang, X.: Characterization
569 of PM_{10} and $PM_{2.5}$ Source Profiles of Fugitive Dust in Zhengzhou, China,
570 AEROSOL AIR QUAL RES, 18, 314-329,
571 https://doi.org/10.4209/aaqr.2017.04.0132, 2018a.
572 Jiang, N., Duan, S., Yu, X., Zhang, R., and Wang, K.: Comparative major components
573 and health risks of toxic elements and polycyclic aromatic hydrocarbons of $PM_{2.5}$
574 in winter and summer in Zhengzhou: Based on three-year data, ATMOS RES, 213,
575 173-184, https://doi.org/10.1016/j.atmosres.2018.06.008, 2018b.
576 Jiang, N., Li, Q., Su, F., Wang, Q., Yu, X., Kang, P., Zhang, R., and Tang, X.:
577 Chemical characteristics and source apportionment of $PM_{2.5}$ between heavily
578 polluted days and other days in Zhengzhou, China, J. Environ. Sci (China), 66,
579 188-198, https://doi.org/10.1016/j.jes.2017.05.006, 2018c.
580 Jiang, N., Wang, K., Yu, X., Su, F., Yin, S., Li, Q., and Zhang, R.: Chemical
581 characteristics and source apportionment by two receptor models of size-segregated

© Author(s) 2019. CC BY 4.0 License.

582 aerosols in an emerging megacity in China, AEROSOL AIR QUAL RES, 18,
583 1375–1390, https://doi.org/10.4209/aaqr.2017.10.0413, 2018d.
584 Jiang, N., Yin, S., Guo, Y., Li, J., Kang, P., Zhang, R., and Tang, X.: Characteristics of
585 mass concentration, chemical composition, source apportionment of $PM_{2.5}$ and
586 PM_{10} and health risk assessment in the emerging megacity in China, ATMOS
587 POLLUT RES, 9, 2367–2380, https://doi.org/10.1016/j.apr.2017.07.005, 2018e.
588 Jiang, N., Li, L., Wang, S., Li, Q., Dong, Z., Duan, S., Zhang, R., and Li, S.: Variation
589 tendency of pollution characterization, sources, and health risks of $PM_{2.5}$-bound
590 polycyclic aromatic hydrocarbons in an emerging megacity in China: Based on
591 three-year data, ATMOS RES, 217, 81-92,
592 https://doi.org/10.1016/j.atmosres.2018.10.023, 2019a.
593 Jiang, N., Liu, X., Wang, S., Yu, X., Yin, S., Duan, S., Shenbo, W., Zhang, R., and Li,
594 S.: Pollution characterization, source identification, and health risks of
595 atmospheric-particle-bound heavy metals in PM_{10} and $PM_{2.5}$ at multiple sites in an
596 emerging megacity in the Central Region of China, AEROSOL AIR QUAL RES,
597 19, 247-271, https://doi.org/10.4209/aaqr.2018.07.0275, 2019b.
598 Kurtenbach, R., Becker, K. H., Gomes, J. A. G., Kleffmann, J., Lorzer, J. C., Spittler,
599 M., Wiesen, P., Ackermann, R., Geyer, A., and Platt, U.: Investigations of
600 emissions and heterogeneous formation of HONO in a road traffic tunnel, Atmos.
601 Environ., 35, 3385-3394, https://doi.org/10.1016/s1352-2310(01)00138-8, 2001.
602 Lelieveld, J., Gromov, S., Pozzer, A., and Taraborrelli, D.: Global tropospheric
603 hydroxyl distribution, budget and reactivity, ATMOS CHEM PHYS, 16, 12477-
604 12493, https://doi.org/10.5194/acp-16-12477-2016, 2016.
605 Li, Q., Jiang, N., Yu, X., Dong, Z., Duan, S., Zhang, L., and Zhang, R.: Sources and
606 spatial distribution of PM2.5-bound polycyclic aromatic hydrocarbons in
607 Zhengzhou in 2016, ATMOS RES, 216, 65–75,
608 https://doi.org/10.1016/j.atmosres.2018.09.011, 2019.

https://doi.org/10.5194/acp-2019-916
Preprint. Discussion started: 29 October 2019
© Author(s) 2019. CC BY 4.0 License.

Atmospheric Chemistry and Physics Discussions

609 Li, X., Brauers, T., Häseler, R., Bohn, B., Fuchs, H., Hofzumahaus, A., Holland, F.,
610 Lou, S., Lu, K. D., Rohrer, F., Hu, M., Zeng, L. M., Zhang, Y. H., Garland, R. M.,
611 Su, H., Nowak, A., Wiedensohler, A., Takegawa, N., Shao, M., and Wahner, A.:
612 Exploring the atmospheric chemistry of nitrous acid (HONO) at a rural site in
613 Southern China, ATMOS CHEM PHYS, 12, 1497-1513,
614 https://doi.org/10.5194/acp-12-1497-2012, 2012.
615 Liu, X., Jiang, N., Yu, X., Zhang, R., Li, S., Li, Q., and Kang, P.: Chemical
616 characteristics, sources apportionment, and risk assessment of PM2.5 in different
617 functional areas of an emerging megacity in China, AEROSOL AIR QUAL RES,
618 19, 2222-2238, https://doi.org/10.4209/aaqr.2019.02.0076, 2019.
619 Liu, Z., Wang, Y., Costabile, F., Amoroso, A., Zhao, C., Huey, L. G., Stickel, R., Liao,
620 J., and Zhu, T.: Evidence of aerosols as a media for rapid daytime HONO
621 production over China, Environ. Sci. Technol., 48, 14386-14391,
622 https://doi.org/10.1021/es504163z, 2014.
623 Markovic, M. Z., VandenBoer, T. C., and Murphy, J. G.: Characterization and
624 optimization of an online system for the simultaneous measurement of atmospheric
625 water-soluble constituents in the gas and particle phases, J. Environ. Monit., 14,
626 1872-1884, https://doi.org/10.1039/c2em00004k, 2012.
627 Michoud, V., Colomb, A., Borbon, A., Miet, K., Beekmann, M., Camredon, M.,
628 Aumont, B., Perrier, S., Zapf, P., Siour, G., Ait-Helal, W., Afif, C., Kukui, A.,
629 Furger, M., Dupont, J. C., Haeffelin, M., and Doussin, J. F.: Study of the unknown
630 HONO daytime source at a European suburban site during the MEGAPOLI
631 summer and winter field campaigns, ATMOS CHEM PHYS, 14, 2805-2822,
632 https://doi.org/10.5194/acp-14-2805-2014, 2014.
633 Pinto, J. P., Dibb, J., Lee, B. H., Rappenglück, B., Wood, E. C., Levy, M., Zhang, R.
634 Y., Lefer, B., Ren, X. R., Stutz, J., Tsai, C., Ackermann, L., Golovko, J., Herndon,
635 S. C., Oakes, M., Meng, Q. Y., Munger, J. W., Zahniser, M., and Zheng, J.:
636 Intercomparison of field measurements of nitrous acid (HONO) during the SHARP

https://doi.org/10.5194/acp-2019-916
Preprint. Discussion started: 29 October 2019
© Author(s) 2019. CC BY 4.0 License.

campaign, J. Geophys. Res., 119, 5583-5601, https://doi.org/10.1002/2013jd020287, 2014.

Qin, M., Xie, P., Su, H., Gu, J., Peng, F., Li, S., Zeng, L., Liu, J., Liu, W., and Zhang, Y.: An observational study of the HONO–NO_2 coupling at an urban site in Guangzhou City, South China, Atmos. Environ., 43, 5731-5742, https://doi.org/10.1016/j.atmosenv.2009.08.017, 2009.

Rappenglück, B., Lubertino, G., Alvarez, S., Golovko, J., Czader, B., and Ackermann, L.: Radical precursors and related species from traffic as observed and modeled at an urban highway junction, J AIR WASTE MANAGE, 63, 1270-1286, https://doi.org/10.1080/10962247.2013.822438, 2013.

Rohrer, F., and Berresheim, H.: Strong correlation between levels of tropospheric hydroxyl radicals and solar ultraviolet radiation, Nature, 442, 184-187, https://doi.org/10.1038/nature04924, 2006.

Sörgel, M., Regelin, E., Bozem, H., Diesch, J. M., Drewnick, F., Fischer, H., Harder, H., Held, A., Hosaynali-Beygi, Z., Martinez, M., and Zetzsch, C.: Quantification of the unknown HONO daytime source and its relation to NO_2, ATMOS CHEM PHYS, 11, 10433-10447, https://doi.org/10.5194/acp-11-10433-2011, 2011.

Shen, L. J., and Zhang, Z. F.: Heterogeneous Reactions of NO_2 on the Surface of Black Carbon, PROG CHEM, 25, 28-35, 2013.

Spataro, F., Ianniello, A., Esposito, G., Allegrini, I., Zhu, T., and Hu, M.: Occurrence of atmospheric nitrous acid in the urban area of Beijing (China), Sci. Total Environ., 447, 210-224, https://doi.org/10.1016/j.scitotenv.2012.12.065, 2013.

Stutz, J.: Nitrous acid formation in the urban atmosphere: Gradient measurements of NO_2 and HONO over grass in Milan, Italy, J. Geophys. Res., 107, https://doi.org/10.1029/2001jd000390, 2002.

Stutz, J., Alicke, B., Ackermann, R., Geyer, A., Wang, S., White, A. B., Williams, E. J., Spicer, C. W., and Fast, J. D.: Relative humidity dependence of HONO

https://doi.org/10.5194/acp-2019-916
Preprint. Discussion started: 29 October 2019
© Author(s) 2019. CC BY 4.0 License.

Atmospheric Chemistry and Physics Discussions

664 chemistry in urban areas, J. Geophys. Res., 109, 03307-03319,
665 https://doi.org/10.1029/2003jd004135, 2004.
666 Su, H., Cheng, Y. F., Cheng, P., Zhang, Y. H., Dong, S., Zeng, L. M., Wang, X.,
667 Slanina, J., Shao, M., and Wiedensohler, A.: Observation of nighttime nitrous acid
668 (HONO) formation at a non-urban site during PRIDE-PRD2004 in China, Atmos.
669 Environ., 42, 6219-6232, https://doi.org/10.1016/j.atmosenv.2008.04.006, 2008a.
670 Su, H., Cheng, Y. F., Shao, M., Gao, D. F., Yu, Z. Y., Zeng, L. M., Slanina, J., Zhang,
671 Y. H., and Wiedensohler, A.: Nitrous acid (HONO) and its daytime sources at a
672 rural site during the 2004 PRIDE-PRD experiment in China, J. Geophys. Res., 113,
673 D14312-14321, https://doi.org/10.1029/2007jd009060, 2008b.
674 Tian, Y., Xue, Q., Xiao, Z., Chen, K., and Feng, Y.: PMF-GAS Methods to Estimate
675 Contributions of Sources and Oxygen for $PM_{2.5}$, Based on Highly Time-Resolved
676 PM2.5 Species and Gas Data, AEROSOL AIR QUAL RES, 18, 2956-2966,
677 https://doi.org/10.4209/aaqr.2018.07.0244, 2018.
678 Tong, S., Hou, S., Zhang, Y., Chu, B., Liu, Y., He, H., Zhao, P., and Ge, M.:
679 Comparisons of measured nitrous acid (HONO) concentrations in a pollution
680 period at urban and suburban Beijing, in autumn of 2014, SCI CHINA CHEM, 58,
681 1393-1402, https://doi.org/10.1007/s11426-015-5454-2, 2015.
682 Vogel, B., Vogel, H., Kleffmann, J., and Kurtenbach, R.: Measured and simulated
683 vertical profiles of nitrous acid—Part II. Model simulations and indications for a
684 photolytic source, Atmos. Environ., 37, 2957-2966, https://doi.org/10.1016/s1352-
685 2310(03)00243-7, 2003.
686 Wang, S., Zhou, R., Zhao, H., Wang, Z., Chen, L., and Zhou, B.: Long-term
687 observation of atmospheric nitrous acid (HONO) and its implication to local NO_2
688 levels in Shanghai, China, Atmos. Environ., 77, 718-724,
689 https://doi.org/10.1016/j.atmosenv.2013.05.071, 2013.
690 Wang, S., Yin, S., Zhang, R., Yang, L., Zhao, Q., Zhang, L., Yan, Q., Jiang, N., and
691 Tang, X.: Insight into the formation of secondary inorganic aerosol based on high-

© Author(s) 2019. CC BY 4.0 License.

692 time-resolution data during haze episodes and snowfall periods in Zhengzhou,
693 China, Sci. Total Environ., 660, 47-56,
694 https://doi.org/10.1016/j.scitotenv.2018.12.465, 2019.
695 Winer, A. M., and Biermann, H. W.: Long pathlength differential optical absorption
696 spectroscopy (DOAS) measurements of gaseous HONO, NO_2 and HCNO in the
697 California South Coast Air Basin, Res. Chem. Intermed., 20, 423-445,
698 https://doi.org/10.1163/156856794X00405, 1994.
699 Wojtal, P., Halla, J. D., and McLaren, R.: Pseudo steady states of HONO measured in
700 the nocturnal marine boundary layer: a conceptual model for HONO formation on
701 aqueous surfaces, ATMOS CHEM PHYS, 11, 3243-3261,
702 https://doi.org/10.5194/acp-11-3243-2011, 2011.
703 Xu, Z., Wang, T., Wu, J., Xue, L., Chan, J., Zha, Q., Zhou, S., Louie, P. K. K., and
704 Luk, C. W. Y.: Nitrous acid (HONO) in a polluted subtropical atmosphere:
705 Seasonal variability, direct vehicle emissions and heterogeneous production at
706 ground surface, Atmos. Environ., 106, 100-109,
707 https://doi.org/10.1016/j.atmosenv.2015.01.061, 2015.
708 Yang, Q., Su, H., Li, X., Cheng, Y., Lu, K., Cheng, P., Gu, J., Guo, S., Hu, M., Zeng,
709 L., Zhu, T., and Zhang, Y.: Daytime HONO formation in the suburban area of the
710 megacity Beijing, China, SCI CHINA CHEM, 57, 1032-1042,
711 https://doi.org/10.1007/s11426-013-5044-0, 2014.
712 Zhang, W., Tong, S., Ge, M., An, J., Shi, Z., Hou, S., Xia, K., Qu, Y., Zhang, H., Chu,
713 B., Sun, Y., and He, H.: Variations and sources of nitrous acid (HONO) during a
714 severe pollution episode in Beijing in winter 2016, Sci. Total Environ., 648, 253-
715 262, https://doi.org/10.1016/j.scitotenv.2018.08.133, 2019.
716

https://doi.org/10.5194/acp-2019-916
Preprint. Discussion started: 29 October 2019
© Author(s) 2019. CC BY 4.0 License.

Atmospheric Chemistry and Physics Discussions

Figure Captions:

Fig. 1. Temporal trends of hourly average T, RH, WD, WS, and $PM_{2.5}$ during the measurement. (The shaded areas : white for the CD period; black for the PD period; red for the SPD period.)

Fig. 2. Temporal variations of hourly average HONO, NO, NO_2, O_3, and CO during the measurement. (The shaded areas : white for the CD period; black for the PD period; red for the SPD period.)

Fig. 3. Diurnal variations of HONO, NO, NO_2, O_3, HONO/NO_2, and HONO/NO_X. The blue points and lines represented the CD period; the black points and lines represented the PD period; the red points and lines represented the SPD period.

Fig. 4. Nocturnal variations of $\mathbf{P}_{\mathbf{OH+NO}}^{\mathbf{net}}$, HONO and NO during CD, PD and SPD periods.

Fig. 5. Percentage distribution of the nighttime $HONO_{emission}$/HONO. (The dotted line represents the average of $HONO_{emission}$/HONO.)

Fig. 6. Nighttime correlation studies between $PM_{2.5}$ and HONO/NO_2, $PM_{2.5}$ and HONO, CO and HONO, RH and HONO/NO_2 during the entire measurement period, CD, PD, and SPD periods. The blue represented the full measurement period; the light blue represented CD period; the black represented PD period; the red represented SPD period.

Fig. 7. Nocturnal variations of $HONO_{correct}$, NO_2, and $HONO_{correct}/NO_2$ in CD, PD and SPD periods.

Fig. 8. The average profiles of J_{HONO} and J_{O^1D} concentrations during the daytime, and production and loss rate of the daytime HONO in CD, PD and SPD periods.

https://doi.org/10.5194/acp-2019-916
Preprint. Discussion started: 29 October 2019
© Author(s) 2019. CC BY 4.0 License.

Atmospheric Chemistry and Physics Discussions

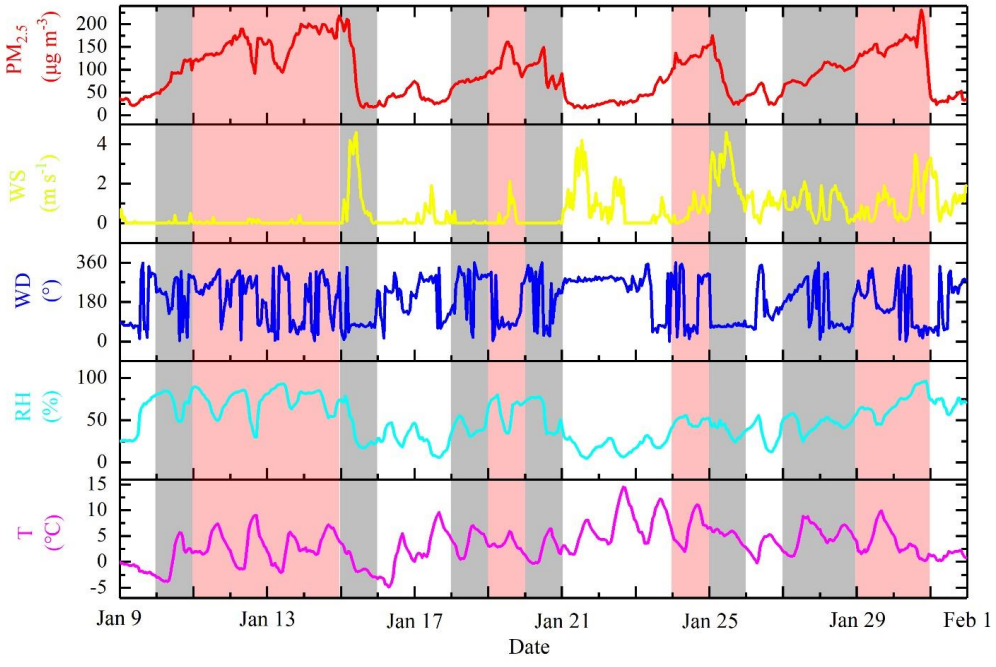

Fig. 1. Temporal trends of hourly average T, RH, WD, WS, and $PM_{2.5}$ during the measurement. (The shaded areas: white for the CD period; black for the PD period; red for the SPD period.)

https://doi.org/10.5194/acp-2019-916
Preprint. Discussion started: 29 October 2019
© Author(s) 2019. CC BY 4.0 License.

Atmospheric Chemistry and Physics Discussions

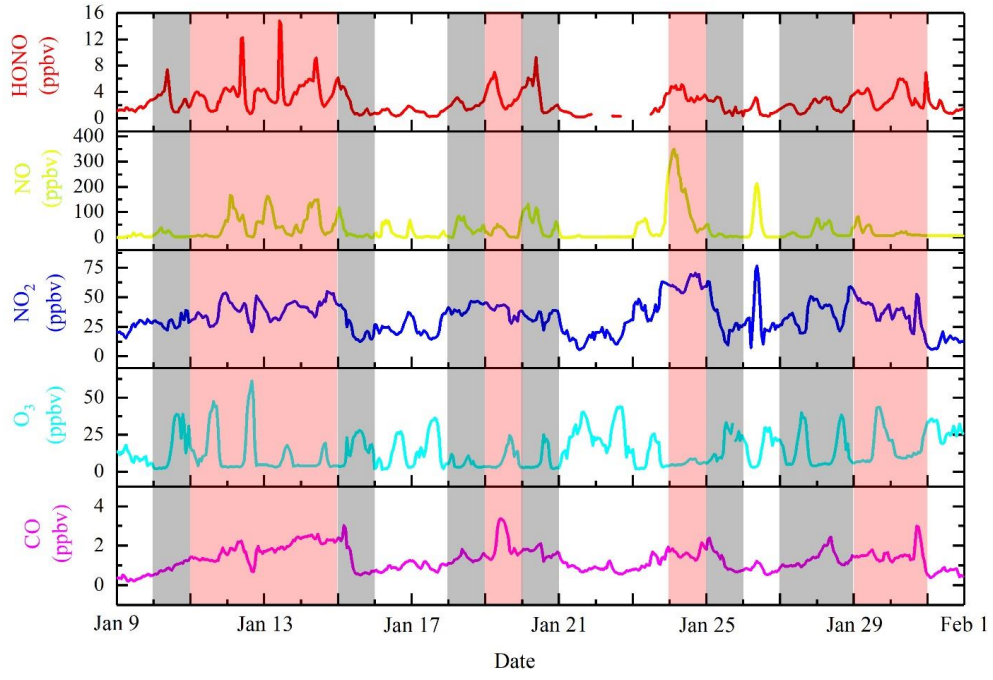

Fig. 2. Temporal variations of hourly average HONO, NO, NO_2, O_3, and CO during the measurement. (The shaded areas: white for the CD period; black for the PD period; red for the SPD period.)

https://doi.org/10.5194/acp-2019-916
Preprint. Discussion started: 29 October 2019
© Author(s) 2019. CC BY 4.0 License.

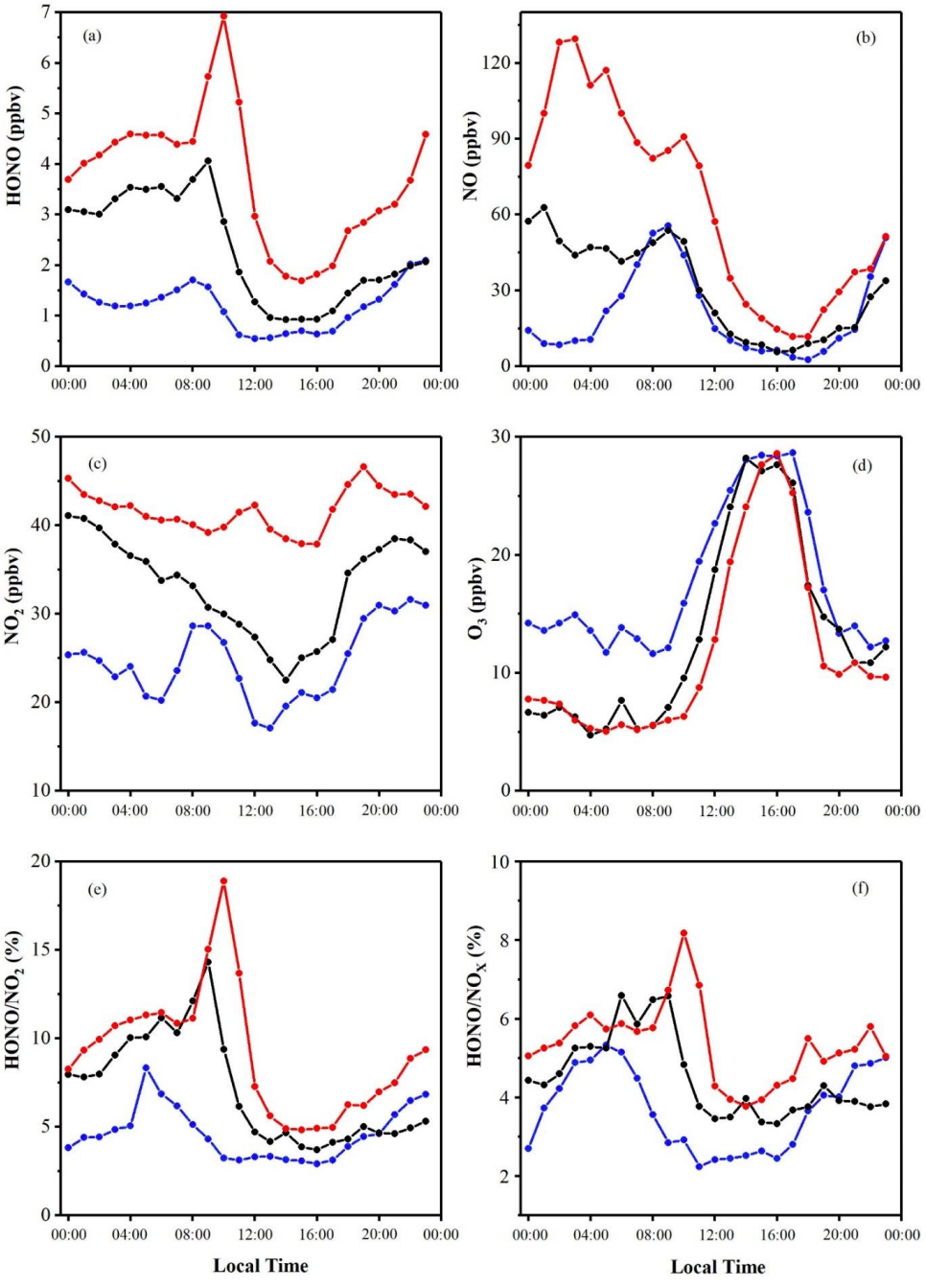

Fig. 3. Diurnal variations of HONO, NO, NO_2, O_3, $HONO/NO_2$, and $HONO/NO_X$. The blue points and lines represented the CD period; the black points and lines represented the PD period; the red points and lines represented the SPD period.

https://doi.org/10.5194/acp-2019-916
Preprint. Discussion started: 29 October 2019
© Author(s) 2019. CC BY 4.0 License.

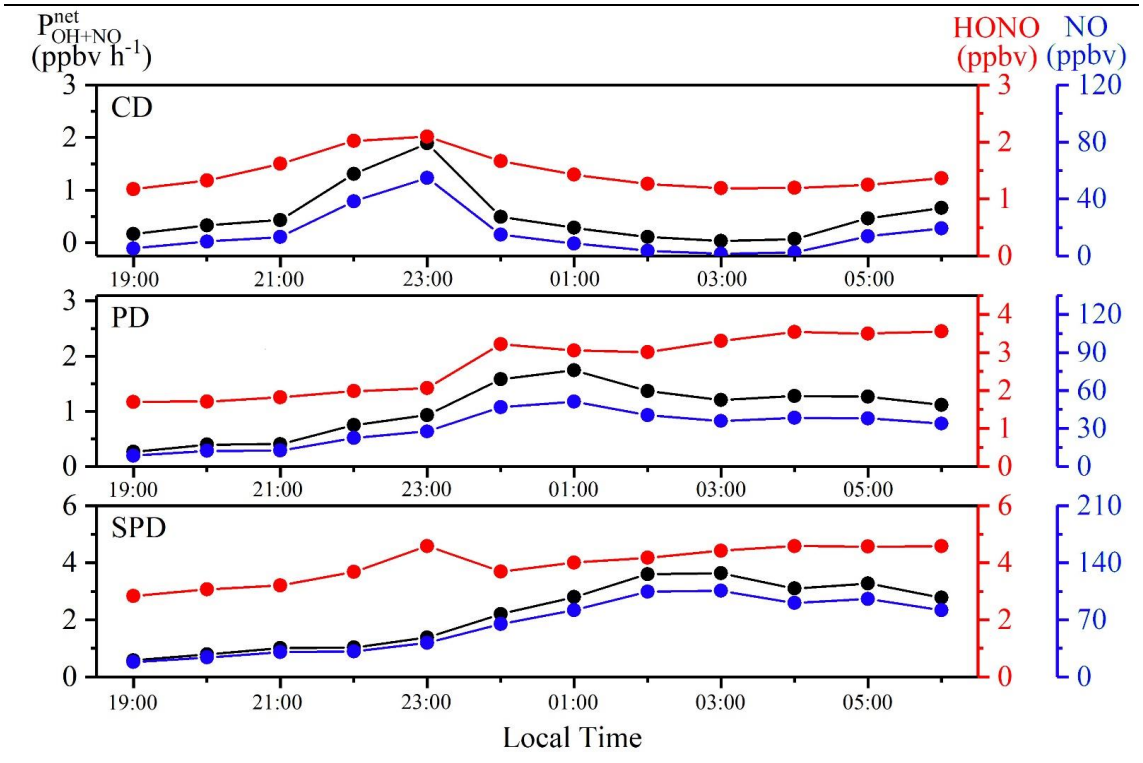

Fig. 4. Nocturnal variations of $\mathbf{P^{net}_{OH+NO}}$, HONO and NO during CD, PD and SPD periods.

https://doi.org/10.5194/acp-2019-916
Preprint. Discussion started: 29 October 2019
© Author(s) 2019. CC BY 4.0 License.

Atmospheric Chemistry and Physics Discussions

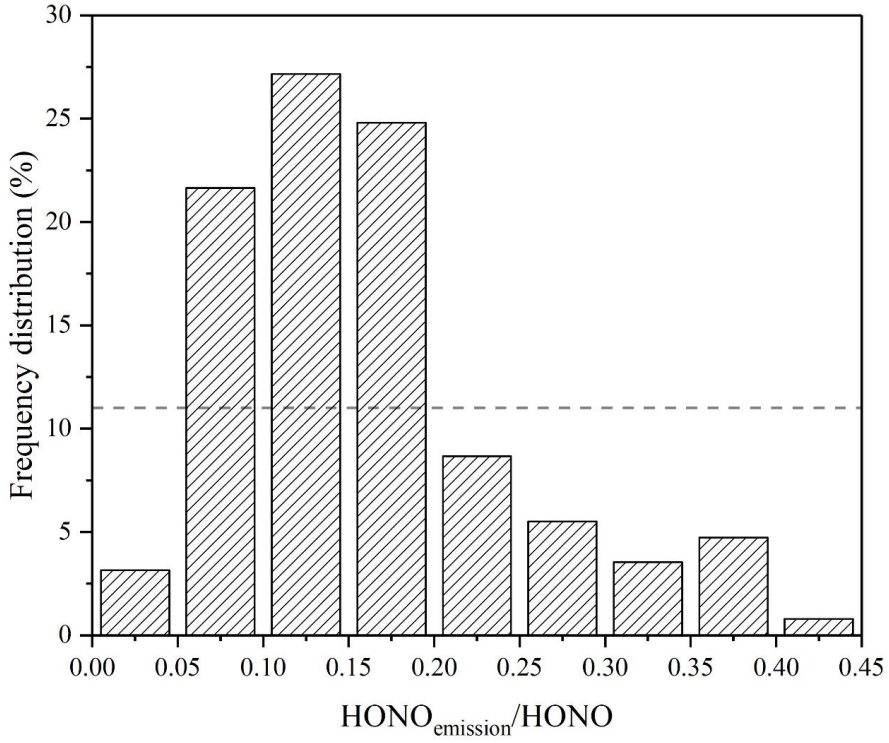

Fig. 5. Percentage distribution of the nighttime $HONO_{emission}/HONO$. (The dotted line represents the average of $HONO_{emission}/HONO$.)

https://doi.org/10.5194/acp-2019-916
Preprint. Discussion started: 29 October 2019
© Author(s) 2019. CC BY 4.0 License.

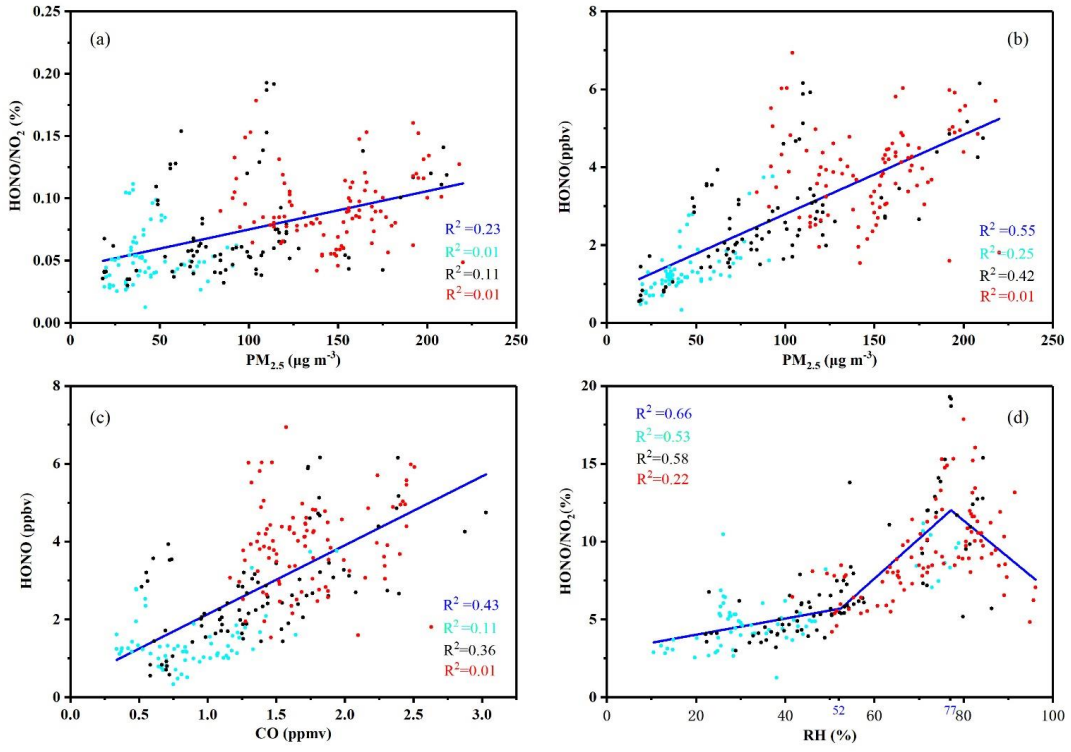

Fig. 6. Nighttime correlation studies between $PM_{2.5}$ and $HONO/NO_2$, $PM_{2.5}$ and HONO, CO and HONO, RH and $HONO/NO_2$ during the entire measurement period, CD, PD, and SPD periods. The blue represented the full measurement period; the light blue represented CD period; the black represented PD period; the red represented SPD period.

https://doi.org/10.5194/acp-2019-916
Preprint. Discussion started: 29 October 2019
© Author(s) 2019. CC BY 4.0 License.

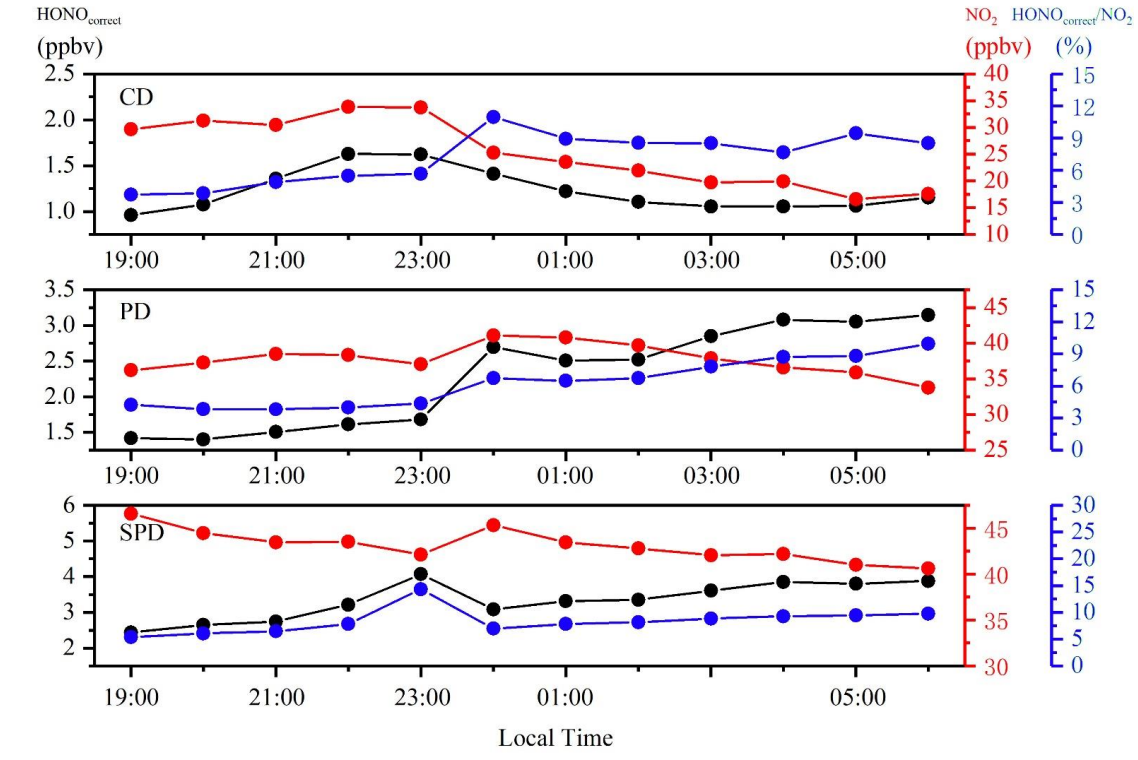

Fig. 7. Nocturnal variations of $HONO_{correct}$, NO_2, and $HONO_{correct}/NO_2$ in CD, PD and SPD periods.

https://doi.org/10.5194/acp-2019-916
Preprint. Discussion started: 29 October 2019
© Author(s) 2019. CC BY 4.0 License.

Atmospheric Chemistry and Physics Discussions

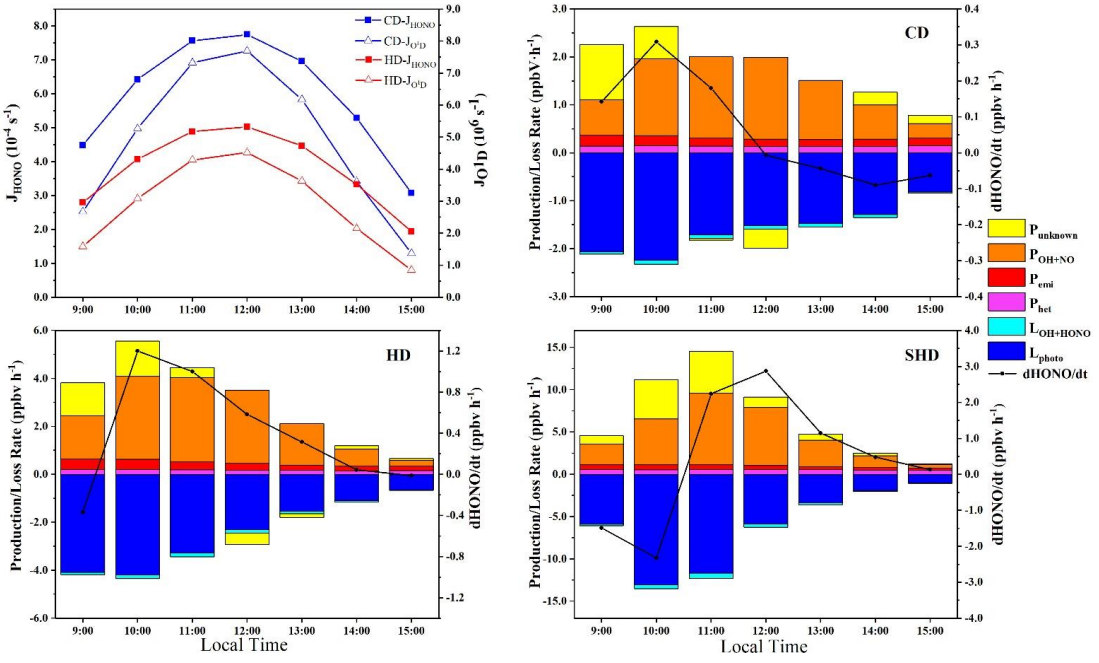

Fig. 8. The average profiles of J_{HONO} and J_{O^1D} concentrations during the daytime, and production and loss rate of the daytime HONO in CD, PD and SPD periods.

https://doi.org/10.5194/acp-2019-916
Preprint. Discussion started: 29 October 2019
© Author(s) 2019. CC BY 4.0 License.

Atmospheric Chemistry and Physics Discussions

Table Captions:

Table 1. Comparisons of the daytime and nighttime HONO level, $HONO/NO_2$, and $HONO/NO_X$ mean values in Zhengzhou and other sites around the world.

Table 2. Data statistics of HONO, $PM_{2.5}$, NO_2, NO, NO_X, $HONO/NO_2$, $HONO/NO_X$, O_3, CO, T, RH, WS and WD during the measurement period, mean value ± standard deviation.

https://doi.org/10.5194/acp-2019-916
Preprint. Discussion started: 29 October 2019
© Author(s) 2019. CC BY 4.0 License.

Atmospheric Chemistry and Physics Discussions

Table 1.

Comparisons of the daytime and nighttime HONO level, $HONO/NO_2$, and $HONO/NO_X$ mean values in Zhengzhou and other sites around the world.

Date (Site)	Instrument	HONO (ppbV)			$HONO/NO_2$ (%)		$HONO/NO_X$(%)		Reference
		Day	Night	N/D	Day	Night	Day	Night	
Oct.–Nov. 2014 (Beijing)	LOPAP (long path absorption photometer)	0.9	1.8	2.0	2.6	4.6	1.7	2.2	Tong et al., 2015
Feb.–Mar. 2014 (Beijing)	LOPAP	1.8	2.1	1.2	3.8 (Severe haze)	4.3	2.5	2.5	Hou et al., 2016
		0.5	0.9	1.8	7.8 (Clean)	3.0	5.1	2.4	
Jul. 2006 (Guangzhou)	LOPAP	0.2	0.9	4.5	1.0	2.5	4.3	4.5	Li et al., 2012
Jul.–Aug. 2015 (Xi'an)	LOPAP	0.5	1.6	3.2	3.3	6.2			Huang et al., 2017
Aug. 2010–Jun.2012 (Shanghai)	Active DOAS	0.8	1.1	1.4	4.2	4.5			Wang et al., 2013
Jul. 2009 (Paris)	Nitro-MAC (A Wet Chemical Derivatization Technique)	0.1	0.2	2.0	3.3	2.5			Michoud et al., 2014
Jun.-Jul. 2005 (Germany)	LP-DOAS	0.1	0.3	3.0	4.1	5.7	1.4	2.1	Elshorbany et al., 2012
Jan. 2019	AIM	2.2	2.8	1.3	6.8	8.5	4.4	5.5	This study

https://doi.org/10.5194/acp-2019-916
Preprint. Discussion started: 29 October 2019
© Author(s) 2019. CC BY 4.0 License.

Table 2.

Data statistics of HONO, $PM_{2.5}$, NO_2, NO, NO_X, $HONO/NO_2$, $HONO/NO_X$, O_3, CO, T, RH, WS and WD during the measurement period, mean value ± standard deviation.

Trace gases	CD			PD			SPD			Total days
	Day	Night	All	Day	Night	All	Day	Night	All	
$PM_{2.5}$ ($\mu g \cdot m^{-3}$)	36.8 ± 15.2	40.7 ± 16.8	38.7 ± 16.1	80.3 ± 31.8	93.3 ± 46	86.8 ± 39.8	147.5 ± 29.1	146.7 ± 33.0	147.1 ± 31.0	91.1 ± 54.4
HONO (ppbV)	0.9 ± 0.7	1.4 ± 0.7	1.1 ± 0.7	1.9 ± 1.7	2.7 ± 1.3	2.3 ± 1.5	3.5 ± 2.7	4.0 ± 1.1	3.7 ± 2.1	2.5 ± 1.9
CO (ppmV)	0.8 ± 0.3	0.8 ± 0.3	0.8 ± 0.3	1.2 ± 0.4	1.4 ± 0.6	1.3 ± 0.5	1.8 ± 0.6	1.7 ± 0.4	1.8 ± 0.5	1.3 ± 0.6
NO (ppbV)	18.4 ± 39.3	15 ± 34.3	16.7 ± 36.8	20.3 ± 26.2	30.7 ± 33.6	25.5 ± 30.4	40.8 ± 50.8	64.3 ± 82.1	52.5 ± 68.9	31.8 ± 51.4
NO_2 (ppbV)	22.8 ± 13	26.4 ± 12.6	24.6 ± 12.9	28.7 ± 9.3	37.8 ± 10.4	33.2 ± 10.8	40.3 ± 11.4	43.1 ± 10.0	41.7 ± 10.8	33.2 ± 13.6
O_3 (ppbV)	21.4 ± 11.5	13.8 ± 10.0	17.6 ± 11.4	17.4 ± 11.9	8.9 ± 8.1	13.1 ± 10.9	15.6 ± 14.2	7.9 ± 7.1	11.8 ± 11.8	14.2 ± 11.7
$HONO/NO_2$ (%)	4.2 ± 3.6	5.3 ± 2.2	4.7 ± 3.1	6.8 ± 5.8	7.4 ± 3.9	7.1 ± 4.9	9.0 ± 7.7	9.8 ± 5.8	9.4 ± 6.8	7.6 ± 6.4
$HONO/NO_X$ (%)	3.3 ± 2.7	6.0 ± 5.6	4.5 ± 4.5	4.4 ± 2.5	4.6 ± 1.7	4.5 ± 2.1	5.3 ± 3.4	5.8 ± 4.7	5.6 ± 4.1	4.9 ± 3.8
RH (%)	29.6 ± 20.9	35.9 ± 19.8	32.8 ± 20.5	43.7 ± 16.9	53.6 ± 17.5	48.6 ± 17.8	64.1 ± 17.8	72.5 ± 12.6	68.3 ± 15.9	49.9 ± 23.5
WS (m/s)	0.8 ± 1.0	0.5 ± 0.7	0.7 ± 0.9	1.1 ± 1.4	0.6 ± 0.9	0.9 ± 1.2	0.4 ± 0.7	0.3 ± 0.6	0.4 ± 0.7	0.6 ± 0.9
T (°C)	4.3 ± 4.6	2.7 ± 3.6	3.5 ± 4.2	3.7 ± 3.3	2.6 ± 3.1	3.1 ± 3.2	4.6 ± 3.2	2.9 ± 2.1	3.8 ± 2.8	3.5 ± 3.5

Atmospheric Chemistry and Physics Discussions
Open Access
EGU